PAPER

Extracting respiratory information from seismocardiogram signals acquired on the chest using a miniature accelerometer

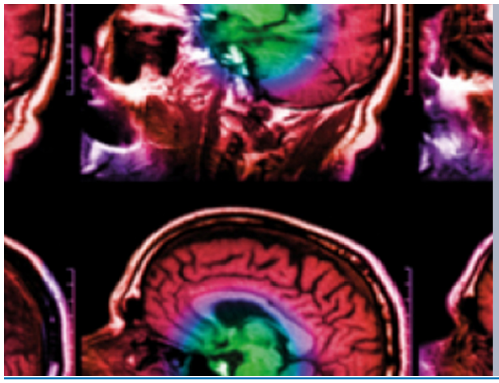

IOP Publishing Physiological Measurement
Physiol. Meas. **33** (2012) 1643–1660 doi:10.1088/0967-3334/33/10/1643

Extracting respiratory information from seismocardiogram signals acquired on the chest using a miniature accelerometer

Keya Pandia[1], **Omer T Inan**[1], **Gregory T A Kovacs**[1,2] **and Laurent Giovangrandi**[1]

[1] Department of Electrical Engineering, Stanford University, Stanford, CA 94305, USA
[2] School of Medicine, Stanford University, Stanford, CA 94305, USA

E-mail: keya.pandia@stanfordalumni.org

Received 3 June 2012, accepted for publication 6 August 2012
Published 18 September 2012
Online at stacks.iop.org/PM/33/1643

Abstract
Seismocardiography (SCG) is a non-invasive measurement of the vibrations of the chest caused by the heartbeat. SCG signals can be measured using a miniature accelerometer attached to the chest, and are thus well-suited for unobtrusive and long-term patient monitoring. Additionally, SCG contains information relating to both cardiovascular and respiratory systems. In this work, algorithms were developed for extracting three respiration-dependent features of the SCG signal: intensity modulation, timing interval changes within each heartbeat, and timing interval changes between successive heartbeats. Simultaneously with a reference respiration belt, SCG signals were measured from 20 healthy subjects and a respiration rate was estimated using each of the three SCG features and the reference signal. The agreement between each of the three accelerometer-derived respiration rate measurements was computed with respect to the respiration rate derived from the reference respiration belt. The respiration rate obtained from the intensity modulation in the SCG signal was found to be in closest agreement with the respiration rate obtained from the reference respiration belt: the bias was found to be 0.06 breaths per minute with a 95% confidence interval of −0.99 to 1.11 breaths per minute. The limits of agreement between the respiration rates estimated using SCG (intensity modulation) and the reference were within the clinically relevant ranges given in existing literature, demonstrating that SCG could be used for both cardiovascular and respiratory monitoring. Furthermore, phases of each of the three SCG parameters were investigated at four instances of a respiration cycle—start inspiration, peak inspiration, start expiration, and peak expiration—and during breath hold (apnea). The phases of the three SCG

parameters observed during the respiration cycle were congruent with existing literature and physiologically expected trends.

Keywords: accelerometer, cardio-respiratory physiology, non-invasive monitoring, respiration rate, apnea

(Some figures may appear in colour only in the online journal)

Introduction

The chest-accelerometry signal contains an ultra-low frequency component corresponding to the motion of the chest wall and a higher frequency seismocardiogram (SCG) component corresponding to vibrations of the chest caused by the heartbeat. The seismocardiogram (SCG) signal offers a non-invasive means of assessing cardiovascular status by measuring the vibrations of the chest caused by the heartbeat (Zanetti and Salerno 1991). SCG sensors used to measure these vibrations can be as simple and unobtrusive as a small, wireless accelerometer patch worn on the chest or through fabric (Castiglioni *et al* 2007), making seismocardiography an appealing choice for monitoring sleep quality (Morillo *et al* 2010), cardiorespiratory status in a hospital bed (Woodward *et al* 2007), or any other applications where it is critical not to reduce the patient's comfort while monitoring the heart.

While the SCG contains both cardiovascular and respiratory diagnostic information, most SCG studies to date have focused on the cardiovascular aspects of the signal. Salerno and Zanetti (1991) showed that SCG signals measured from the sternum are stable over the course of months and capable of detecting acute or chronic changes in left ventricular function. Castiglioni *et al* (2007) demonstrated that sternal SCG signals can be decomposed into low-frequency ($<$20 Hz) components relating to cardiac output, and higher-frequency ($>$20 Hz) components originating from the heart sounds.

The studies that have investigated the respiratory aspects of SCG measurements have primarily focused on the ultra-low frequency ($<$1 Hz) fluctuations of the signal caused by the movement of the chest wall (Morillo *et al* 2010, Reinvuo *et al* 2006). These approaches focusing on chest wall movement alone do not consider any amplitude-, timing-, or morphology-based changes in the SCG signal that are caused by the respiratory cycle. In 2008, Tavakolian *et al* did examine the morphological changes in the SCG[3] signal caused by respiration in the context of improving the procedure for averaging SCG heartbeats, but did not explore the specific changes in the signal nor explain the underlying physiological mechanisms for these changes.

This paper closely examines the effects of respiration on the SCG signal, focusing on methods for extracting specific respiration-dependent features of the signal: intensity modulation, timing interval changes within each heartbeat, and timing interval changes between successive heartbeats. In this work, rather than respiration measurement being secondary to cardiovascular monitoring—or a means to improve the quality of the cardiovascular component of the signal—we focused entirely on understanding the effects of respiration on the SCG.

[3] In their paper, Tavakolian *et al* (2008) refer to the signal they are measuring as the ballistocardiogram (BCG), but since then have revised their naming of the signal to the SCG (Tavakolian *et al* 2011).

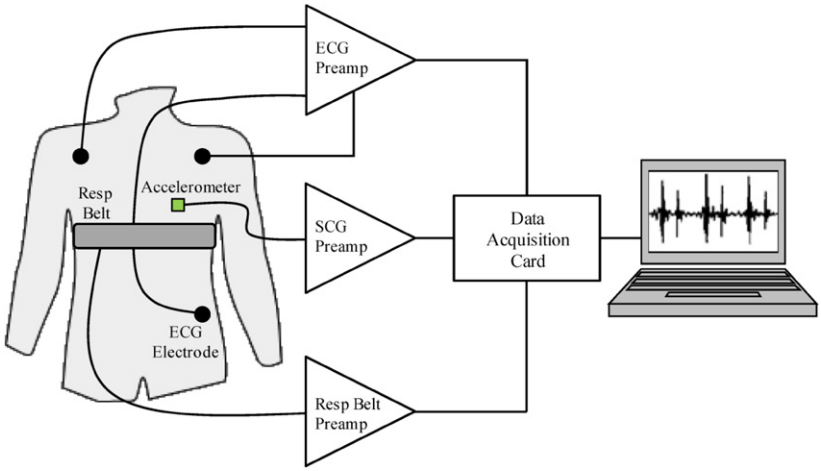

Figure 1. Block diagram of measurement setup. The accelerometer was positioned on the left side of the chest to maximize the heart-sound component of the SCG signal. The respiration belt was used as a reference signal for evaluating the respiration rate estimated from various parameters of the SCG signal. The ECG signal was used for heartbeat detection and segmentation, and could be omitted in future studies with improved S1 peak detection algorithms.

1. Methods

1.1. Measurement system

Figure 1 shows a block diagram of the measurement system. A miniature (0.08 gram, $5 \times 5 \times 1.6\,\text{mm}^3$) triple-axis, low-power, analog-output MEMS accelerometer (LIS3L02AL, STMicroelectronics, Geneva, Switzerland) was attached to the chest of subjects in the left mid-sternal, mid-clavicular region, using clear surgical tape. Although acceleration signals along all three axes were measured, this work focused specifically on the direction most commonly considered as the SCG in the literature—the antero–posterior axis, orthogonal to and into the plane of the chest.

The signal detected by the accelerometer consisted of two main components: (1) a large low-frequency (sub-Hz) component caused by movements of the chest wall due to respiratory expansion and contraction of the lungs; and (2) a component much smaller in amplitude but higher in frequency content (>5 Hz) caused by vibrations of the chest wall due primarily to acoustic waves generated by the heart valves. The aim of the analog front-end was to amplify the latter of these components significantly while not allowing the larger, lower frequency deflections to saturate the electronics. As a result, the signal was high-pass filtered ($f_{-3\,\text{dB}} = 0.3$ Hz), amplified with a gain of 10, and filtered with a fifth-order low-pass anti-aliasing filter (Butterworth, $f_{-3\,\text{dB}} = 1$ kHz). While the high-pass corner frequency of 0.3 Hz did slightly attenuate the low-frequency chest expansion component of the signal, this component still remained sufficiently high in amplitude for all subsequent analysis. The accelerometer signal was then digitized at 10 k samples/s using a data acquisition card (National Instruments, Austin, TX) and custom software (Matlab®, Version 2007b, The Mathworks, Natick, MA).

The reference respiration signal was acquired using a piezoelectric respiration belt (DYmedix, Minneapolis, MN) fastened around the subject's upper torso. The signal was amplified using a simple non-inverting amplifier (gain = 100). A reference (lead-II)

electrocardiogram signal was simultaneously acquired with a custom amplifier (gain = 1000, BW = 0.05–200 Hz).

1.2. Human subject protocol

Twenty healthy volunteers (eight female, twelve male) were recruited at Stanford University. Data from two subjects (one male, one female) were not used for the analysis due to poor reference respiration belt signals. The procedures for collection of human subject data were in accordance with protocol 6503 approved by the Stanford Institutional Review Board (IRB).

The demographics of the recruited subjects were as follows (min-max, mean, standard deviation): age (23–49, 28.9, 5.9 years); height (1.45–1.91, 1.71, 0.11 m); weight (38.6–99.8, 65.9, 12.8 kg); and body mass index (18.1–28.3, 22.3, 2.5). The subjects were each asked to sit in a chair with the accelerometer attached to their chest (in the left, mid-sternal, mid-clavicular area, for reasons explained under section 1.3, sensor positioning below) and the respiration belt fastened around the upper chest. The subjects were then asked to breathe at a comfortable pace for a period of 60 s. A single subject, selected randomly from the 20 subjects recruited for this study, was asked to annotate the start of inspiration cycles with time stamps using the recording software.

The 20 subjects were asked to breathe normally for 60 s, following which, they were asked to hold their breath for 15 s. They were then asked to resume normal breathing for 60 s. The signals from the subjects were plotted and visually inspected to determine the effect of apnea on the signals.

To investigate the effect of intra-subject variability, signals from a single subject (not included in the original 20 subject pool described above) were recorded at four different instances in time. The minimum interval between any two recording instances exceeded 60 days. The subject was asked to breathe normally and the signals were recorded and analyzed.

1.3. Sensor positioning

The SCG signal is composed of multiple components, including features corresponding to the primary heart sounds[4]—S1 and S2—and the lower frequency blood flow induced components as outlined by Castiglioni *et al* (2007). With the primary goal of evaluating left ventricular function, most SCG studies in the existing literature position the accelerometer at the sternum (e.g., Salerno and Zanetti 1991, Tavakolian *et al* 2008).

In contrast, the work presented here aimed to analyze the effects of respiration on the SCG—this includes changes in blood flow and intrathoracic pressures as well as changes in the timing and amplitudes of the hearts sounds. As a result, other positions besides the sternum were also investigated. In comparison with the S1 component of the heart sounds, the S2 component was found to be weaker for most subjects and the strength of the detected S2 component was more sensitive to sensor positioning. Early studies by Agress *et al* (1961) showed that the S2 component is much stronger in the left mid-sternal region of the chest. Accordingly, measurements were taken from three subjects to determine whether this position on the left side of the chest could provide more respiratory information than the typical location on the sternum. As shown in section 2, the position to the left of the sternum was found to

[4] While the terms S1 and S2 primary heart sounds used here to describe features or components of the SCG signal are consistent with literature on phonocardiography (e.g., Lababidi *et al* 1970), it may be noted that the SCG-derived S1 and S2 components, while concurrent in time with the S1 and S2 heart sound components measured on a phonocardiogram, include sub-audible (<20 Hz) frequency components not typically present in a phonocardiogram signal.

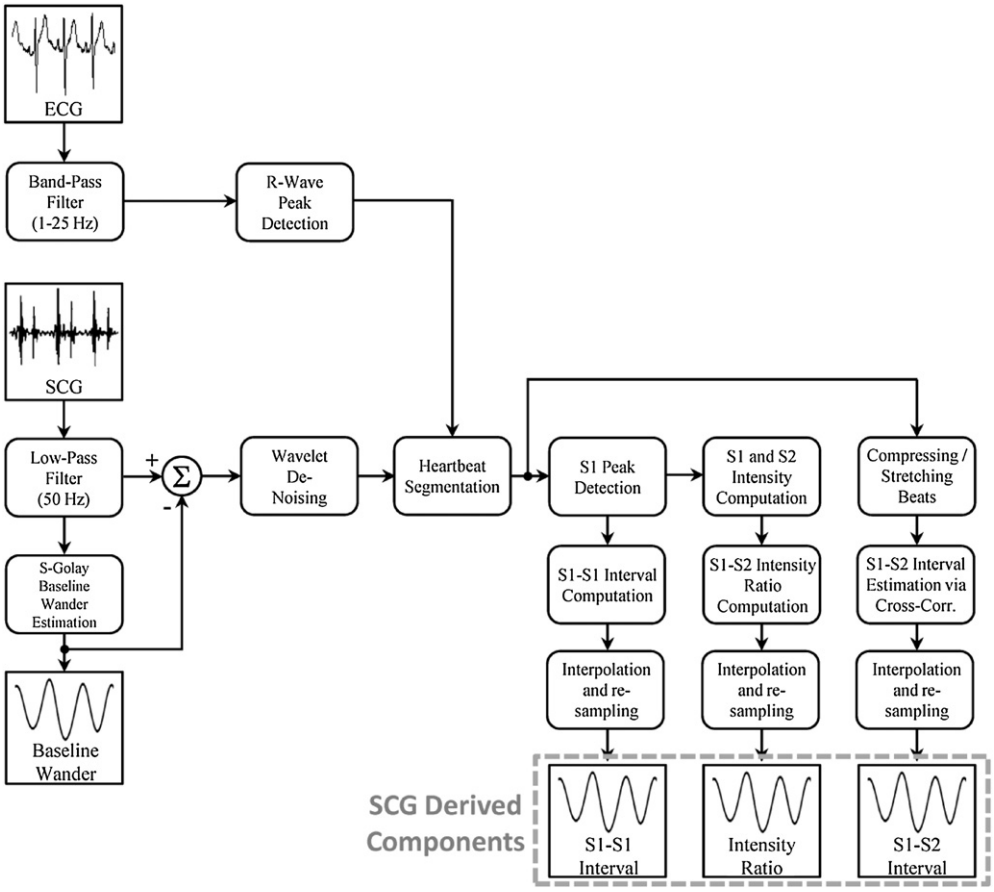

Figure 2. Flowchart showing signal processing steps for extracting three respiration features from the SCG signal.

contain a stronger S2 component than the position on the sternum—consequently, the left mid-sternal, mid-clavicular area was used for all measurements taken in this work.

1.4. Signal processing

1.4.1. Preprocessing and SCG feature extraction. Figure 2 provides a flowchart summarizing the signal processing steps used to extract respiration features from the SCG signal. The chest acceleration signal in the antero–posterior direction corresponding to the SCG was digitally low-pass filtered at 50 Hz. The low-frequency (sub 1 Hz) baseline wander component was removed using Savitzky–Golay polynomial estimation and subtraction (Savitzky and Golay 1964). The filtered SCG signal was then de-noised using a fourth-order Daubechies wavelet (Messer 2001), a 14th-order of decomposition and soft thresholding.

From the reference ECG signal, the R-waves were detected. For each R-wave peak, the maximum amplitude of the SCG signal for the first 100 ms following the R-wave peak was determined to be the S1 peak for the corresponding cardiac cycle. The resulting S1 peaks were used for heartbeat segmentation on the SCG signal. An array of SCG beats was generated, with

each beat in the array spanning a time window starting at 200 ms prior to the corresponding S1 peak location and ending 500 ms after the S1 peak. The time interval between the S1 peak for one beat, and the S1 peak for the previous beat is referred to below as the S1–S1 timing interval.

The root-mean-square (RMS) power of the beat windowed from 200 ms preceding to 150 ms following the S1 peak was considered the intensity of the S1 component and the RMS power of the beat windowed from 220 ms following the S1 peak to the end of the beat was considered the intensity of the S2 component. The ratio of these two intensities was then computed, and is referred to below as the S1–S2 intensity ratio.

1.4.2. S1–S2 interval estimation. The interval between the two primary heart sounds defines the systolic phase of the cardiac cycle (ventricular contraction) (Leighton 1971); the interval from S2 to S1 of the following heartbeat corresponds to the diastolic phase (ventricular filling). Changes in intra-thoracic pressure during respiration modulate venous return and after load, leading to a variation in strength and duration of the ventricular contractions. This ultimately manifests as a change in the interval between the primary S1 and S2 heart sounds. As a result, the S1–S2 timing interval was another feature of the SCG for which respiratory effects were investigated.

Unfortunately, beat-by-beat morphological changes in the SCG and motion-induced artifacts precluded the direct computation of this interval using simple peak detection. Furthermore, traditional approaches used to compare beat-by-beat changes in signal morphology (e.g., ensemble averaging) smooth out many of the higher-frequency features of the signal—in particular, the S2 peak is smoothed due to the beat-by-beat changes in the S1–S2 interval.

For these reasons, a more sophisticated technique was developed for determining S1–S2 timing variations, based on a simplified time-warping algorithm. This algorithm compared one SCG heartbeat to the previous beat to quantify the change in the S1–S2 timing interval. To this end, the SCG signal was segmented into successive heartbeats using reference R-wave peaks (as explained in 1.4.1 above). Each SCG beat (containing both S1 and S2 sounds) was then linearly compressed or stretched (warped) in time, step-wise, by interpolation and re-sampling. Such time warping was performed in steps of 1 ms, within ± 30 ms, thus leading to a set of 60 SCG beats identical in amplitude and morphology, but warped in time. These 60 beats were then each cross-correlated against the non-time-warped previous SCG heartbeat to determine which had the largest cross-correlation with the previous beat—the warping scale at which the largest correlation was found provided the estimate of the S1–S2 timing interval changes. It may be noted that since each pair of consecutive beats is analyzed independently to find the change in S1–S2 interval from one beat to the next, any errors in the estimated S1–S2 intervals do not propagate from one beat pair to the next. Figure 3 shows consecutive SCG heartbeats over one respiratory cycle to illustrate the changes in the S1–S2 interval during the respiratory cycle.

1.5. Analysis

1.5.1. Analysis of individual time-traces. The effects of respiration on each of the three accelerometer-derived parameters—S1–S1 timing interval, S1–S2 intensity ratio, and S1–S2 timing interval—were qualitatively evaluated using time traces from individual subjects. Each of these three features formed a discrete time-series at a varying sampling rate, equal to the instantaneous heart rate, different from the sampling rate of the reference respiration trace. To compare these features to the reference respiration signal, each time-series was interpolated

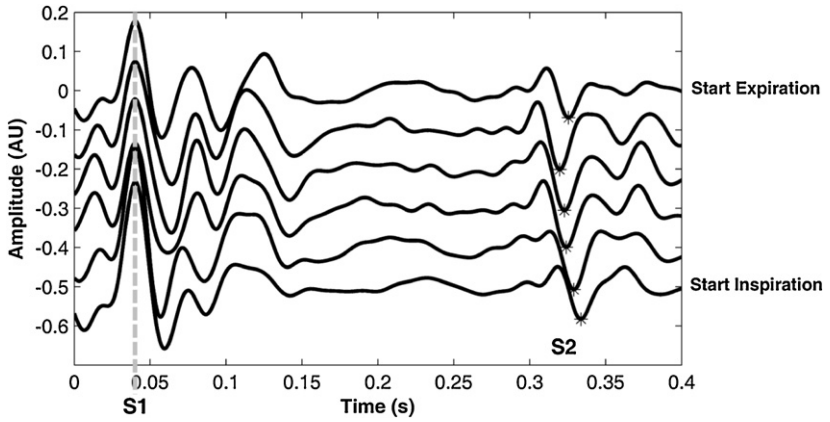

Figure 3. Consecutive cardiac cycles (over one respiration cycle, one subject) superimposed, offset, and aligned to the S1 heart sound timings. Variation in S1–S2 interval is evident from these beats.

linearly at 1 kHz and the ensuing interpolated signal was smoothed using a low-pass filter at 0.4 Hz.

The interpolated SCG signals were plotted alongside the reference respiration signal, and the synchronicity and phase relations were observed during normal breathing. The signals were also plotted for one subject during breath-hold to qualitatively evaluate the effect of apnea on each signal.

1.5.2. Statistical analysis for inter-subject variability. The respiration rate (in breaths per minute (bpm)) was then estimated from each of the three individual signals and compared to the rate estimated from the reference signal. The agreements were assessed using Bland–Altman methods (Bland and Altman 1986). For each signal, time-domain methods using the measurement of auto-correlation peaks were employed to estimate the respiration rate. To this end, an auto-correlation function was applied on a 20 s moving window (0.2 s shift) for each respiration signal. The average interval between the auto-correlation peaks was considered the respiration cycle period and its inverse the respiration rate.

Then, according to Bland–Altman analysis methods, the difference between the SCG-derived and respiration-belt-derived respiration rate was plotted against the mean. The 95% confidence intervals for each of these distributions were computed assuming normality.

A similar statistical analysis was performed on an averaged or aggregate respiration rate derived using all three parameters.

1.5.3. Statistical analysis for intra-subject variability. The Bland–Altman analysis approach described above for analyzing inter-subject variability was also used to analyze the four recordings of a single subject, to investigate intra-subject variability. The agreement between an aggregate respiration rate, obtained from the average of the three accelerometer-derived parameters, and the reference respiration rate, obtained from the respiration belt, was computed for the four recordings of the single subject.

1.5.4. Statistical analysis of respiratory SCG changes according to respiratory phase and apnea. In addition to analyzing the ability of the accelerometer parameters to estimate

respiration rate, the effects of respiration on the three SCG parameters were further analyzed to investigate the effects of respiratory phase and apnea (breath hold). To this effect, variations in the three SCG-derived parameters were quantified along four phases of the respiratory cycle—start inspiration, peak inspiration, start expiration, and peak expiration—as well as during apnea. The respiration waveform derived from each of the three SCG parameters was normalized to a maximum value within the recording, to facilitate inter-subject comparison of phases.

For each subject, a normalized amplitude measure of each of the three SCG parameters was computed at each of the four distinct instances along every respiration cycle of the 60 s of regular breathing. An aggregate (mean) normalized amplitude for each parameter at each of the four respiratory instances was then obtained for each subject. Finally, a single mean normalized amplitude for each parameter at each of the four respiratory instances was computed across all 18 subjects. Similarly, a measure of aggregate (mean) normalized amplitude during the 15 s interval of apnea (breath hold) was obtained for each subject, and then aggregated across 18 subjects.

The aggregate normalized amplitude across the 18 subjects for each of the three SCG parameters—S1–S1 timing interval, S1–S2 intensity ratio and S1–S2 timing interval—along the four phases of the respiration cycle was compared to the normalized amplitude of the respective SCG parameter during apnea to investigate respiratory SCG changes. For this comparison, statistical significance of the changes was assessed using Student's t-test, with a threshold of $p < 0.05$ corrected for multiple comparisons using the Holm–Bonferroni method (Holm 1979).

1.5.5. Effects of heart-rate on respiration rate estimation. Since the SCG-derived parameters rely on reconstructing the respiration waveform based on discrete samples taken every heartbeat, there may exist a risk analogous to aliasing (Shannon 1949). With less than or equal to two data points (cardiac cycles) per respiration cycle, the reconstruction of the continuous respiration waveform would theoretically be inaccurate and unreliable. This effect might be especially pronounced for subjects with low resting heart-rate (e.g., bradycardia), or during phases of rapid respiration (e.g., exercise). In this study, the ratio of heart rate to respiration rate was always higher than two, such that Nyquist-based sampling rate requirements were always met. Furthermore, the effects of heart rate on respiration rate estimation outside of aliasing were quantified as follows: a composite respiration rate derived from an average of all three SCG-derived parameters was computed, and the error in this rate compared to the rate estimated from the reference signal was plotted against heart rate.

2. Results and discussion

2.1. Analysis of individual time-traces

As shown in figure 4 and corroborated by Agress *et al* (1961), the S2 heart sound component was found to be stronger with the sensor placed on the left side of the chest, as compared to the sternal sensor placement.

Figure 5 shows the three different respiration-dependent features derived from the SCG alongside the reference respiration trace. For a majority of the subjects, the phase relations observed for the S1–S1 timing interval, S1 and S2 intensity and S1–S2 timing interval with respect to the inspiratory and expiratory phases were consistent with previous findings (Amit *et al* 2009). Overall, as shown in figure 5, the inter-beat S1–S1 interval was found to be lowered during inspiration as reported in previous work on respiratory sinus arrhythmia

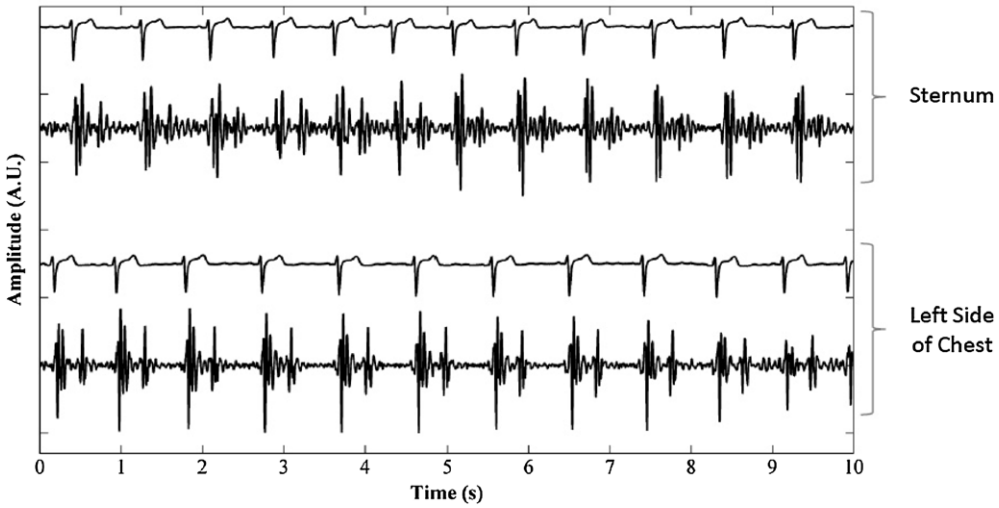

Figure 4. Top: ECG and SCG signals measured at the sternum. Bottom: ECG and SCG signals measured on the left side of the chest, where the heart-sound components of the SCG signal are significantly higher.

(RSA) and heart-rate variability (Berntson *et al* 1993). Furthermore, the power of S1 was attenuated during inspiration and emphasized during expiration; the power of S2 was enhanced during the inspiratory phase. The S1–S2 interval was generally observed to be shorter during the inspiratory respiration phase across subjects—it was observed to be its shortest at late inspiration, early expiration. These trends are in agreement with their underlying physiological causes and mechanisms.

The effect of breath-hold on the three parameters for one of the twenty subjects measured is shown in figure 6. The S1–S1 timing interval exhibits a Valsalva-like pattern of sharp increase followed by gradual decrease, consistent with the parasympathetic effects of breath-hold on the cardiovascular system. For both S1 and S2, the average power during breath-hold was lower than the corresponding average power during normal breathing, with no significant fluctuations. The S1–S2 timing interval was relatively flat for the duration of breath-hold. These results were reproducible across the subjects measured.

2.2. Statistical analysis for respiration rate estimation

Bland–Altman plots for each parameter of respiration compared to the reference signal, across the 18 subjects, are shown in figure 7; corresponding Bland–Altman parameter values (bias, standard deviation and confidence intervals) are listed in table 1. Of all three features derived from the accelerometer signal, the S1–S2 intensity ratio yielded the strongest agreement for respiration-rate measurement.

As shown in figure 7 and table 1, the confidence interval measured for the respiration rate derived from the S1–S2 intensity ratio across the 18 subjects, was found to lie within 1.11 and −0.99 bpm of the reference rate, with a bias of 0.06 bpm. Consequently, strong agreement was observed for inter-subject measurements between the respiration-rate derived from the accelerometer and the reference respiration rate derived from the respiration belt.

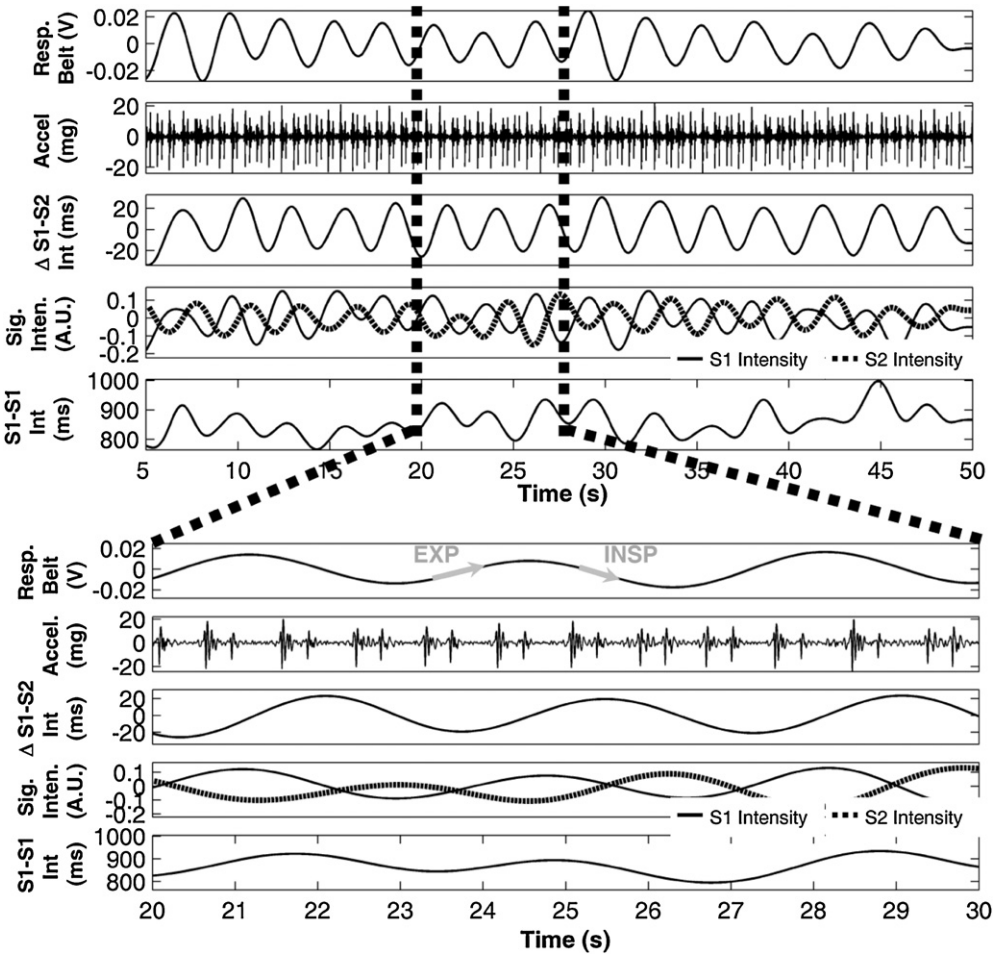

Figure 5. Reference respiration belt signal and raw acceleration signals along with the three respiration-dependent features extracted from the SCG signal over a 60 s recording. Approximate instants of inspiration and expiration over a 10 s breathing period are annotated in the magnified plot—'EXP' corresponds to the point of peak expiration, and 'INSP' corresponds to peak inspiration. These times were recorded by the subject during measurement. S1 and S2 signal intensities shown are normalized intensities.

As shown in figure 8(a), the confidence interval measured for the aggregate respiration rate (simple average), computed from combining the three individual respiration rates across the 18 subjects, was found to lie within 1.38 and −2.22 bpm of the reference rate, with a bias of −0.42 bpm. Consequently, while strong agreement was observed for inter-subject measurements between the aggregate respiration-rate derived from the accelerometer and the reference respiration rate derived from the respiration belt, the aggregate respiration measure did not out-perform the S1–S2 intensity metric for this dataset. It may be noted that signal fusion approaches more sophisticated than the simplistic averaging approach used here may be employed to improve the aggregate respiration rate measurement.

As shown in figure 8(b), the aggregate (simple average) respiration rate computed from the three parameters for an individual subject across four measurement instances spread in

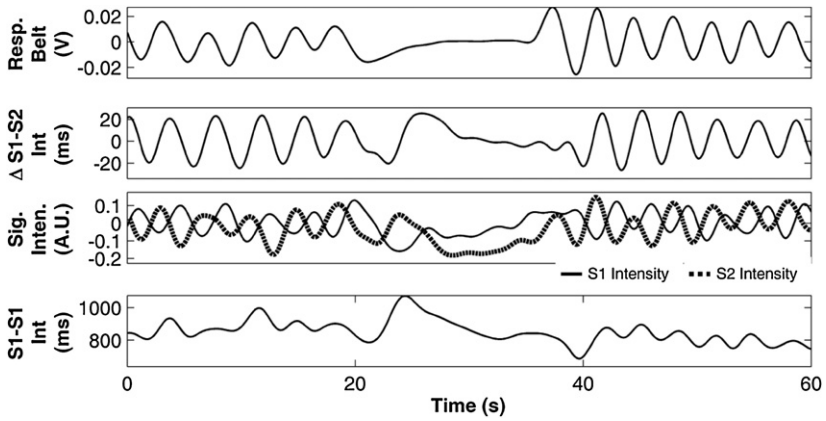

Figure 6. Reference respiration belt signal and the three respiration-dependent features extracted from the SCG signal shown with a period of breath hold. S1 and S2 signal intensities shown are normalized intensities.

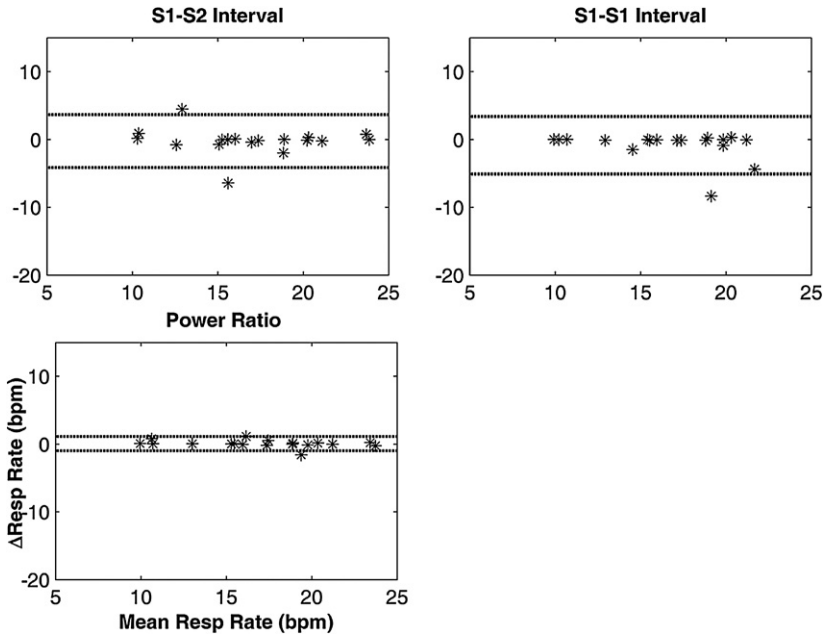

Figure 7. Bland–Altman plots of each of the three respiration-dependent features extracted from the SCG and compared against a respiration belt, across 18 subjects. For all three plots, the units are in breaths per minute (bpm). A tighter (lower) confidence interval in a Bland–Altman plot would correspond to closer agreement with the reference signal.

Table 1. The Bland–Altman values (in breaths per minute) corresponding to bias, standard deviation and confidence intervals for all three accelerometer-derived parameters, across the 18 subjects.

Bland–Altman statistics (bpm)	S1–S2 interval	S1–S1 interval	Signal intensity (power ratio)
Bias	−0.23	−0.85	0.06
Standard deviation	1.99	2.16	0.53
Conf. Int. (+)	3.67	3.38	1.11
Conf. Int. (−)	−4.13	−5.08	−0.99

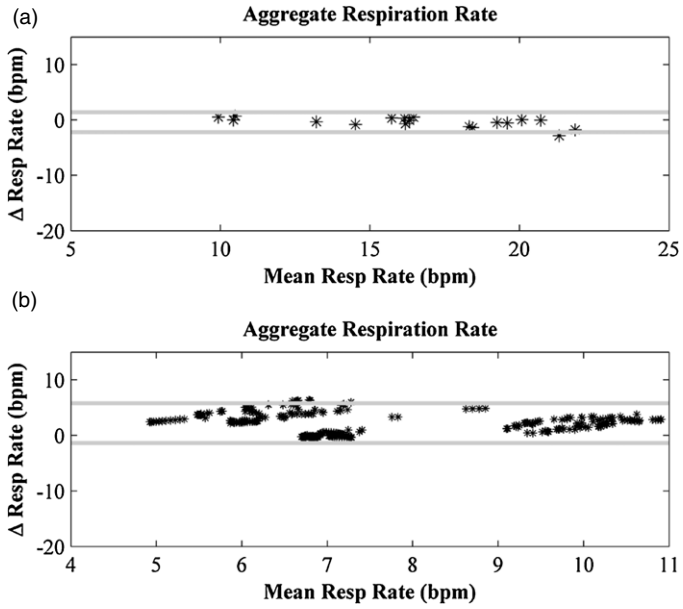

Figure 8. (a) Bland–Altman plots for the aggregate respiration rate computed from the three respiration-dependent features extracted from the SCG and compared against a respiration belt, across 18 subjects. (b) Bland–Altman plot for an aggregate respiration rate computed from the three respiration-dependent features extracted from the accelerometer signal and compared against a respiration belt, across four measurements of a single subject.

time was found to lie within −1.37 and 5.81 bpm of the reference rate, with a bias of 2.22 bpm.

For both inter-subject and intra-subject variability measurements, the limits of agreement fall within the clinically acceptable range shown in published literature of ±4 to ±6 bpm (Droitcour *et al* 2009, Lim *et al* 2002).

2.3. Respiratory SCG changes and underlying physiological mechanisms

2.3.1. Signal intensity modulation. The amplitude and power of the two primary heart sounds—S1 and S2—are modulated by respiration, as is the ratio between their powers. The amplitude and power modulate due to the respiration-dependent variation in the distance between the sound source and the accelerometer.

More importantly, the intensity of the heart sound signal at the source itself varies with respiration. Respiration-induced changes in intra-thoracic pressure cause the ventricular preload and afterload to change, affecting the pressure gradients across which the heart valves close (Sakamoto 1965, Kusukawa 1966). This results in an out-of-phase modulation of the intensity of S1 and S2 sounds (Amit *et al* 2009).

As described by Amit *et al*, during inspiration, pleural pressure decreases resulting in an increased venous return. This causes increased right ventricular preload (end diastolic volume), and a consequent decrease in left ventricular compliance resulting from ventricular interdependence. Decreased left ventricular compliance results in a reduction in left ventricular preload (end diastolic volume) and a reduction in left ventricular force of contraction. This ultimately results in a decreased intensity of the S1 heart sound during inspiration.

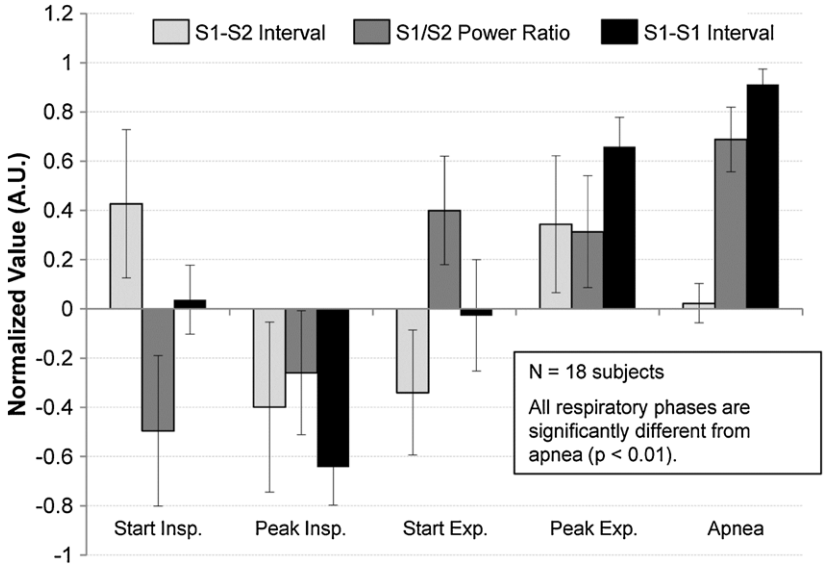

Figure 9. Measure of three SCG parameters (measured relative to amplitude normalized time-traces) at four distinct intervals of a respiration cycle and during apnea, measured across 18 subjects.

Furthermore, an increase in left ventricular afterload during inspiration (arising due to increased arterial resistance), combined with the inspiratory decrease in left ventricular preload (and decreased left ventricular force of contraction), results in an increase in the intensity of the S2 heart sound during inspiration.

As shown in figure 9, the power ratio between SCG-derived S1 and S2 heart sounds is found to diminish during inspiration, indicating a decrease in S1 intensity and a concurrent, out-of-phase increase in S2 intensity during inspiration, in accordance with the above-described physiologically expected trends. This out-of-phase respiratory modulation of S1 and S2 heart sound intensities is also apparent in the time signal for a single subject, as shown in figure 5.

2.3.2. S1–S2 interval. As described above, the interval between S1 and S2 corresponds to the period of ventricular contraction—systole (Leighton 1971); the interval from S2 to S1 (of the following heartbeat) corresponds to ventricular filling—diastole. Changes in intra-thoracic pressure during respiration modulate venous return and after-load, leading to a variation in strength and duration of the ventricular contractions. This ultimately manifests as a change in the interval between the primary S1 and S2 heart sounds.

During inspiration, increased venous return causes an increase in right ventricular preload and a consequent reduction in left ventricular compliance and left ventricular end-diastolic volume (left ventricular preload). This results in a shorter duration of left ventricular systole during inspiration. Conversely, increased left ventricular compliance and left ventricular preload during expiration results in a lengthened left ventricular systole during expiration.

Figure 9 demonstrates that the S1–S2 interval derived from the accelerometer-derived SCG signal is lengthened during peak expiration and early inspiration, indicating a lengthened

systole and a delayed S2 sound (relative to its preceding S1 sound) and the S1–S2 interval is reduced during peak inspiration and early expiration, indicating a shorter systole and an advanced S2 sound (relative to its preceding S1 sound). These findings are congruent with previous studies (Amit *et al* 2009) and the above-described physiologically expected trends. This respiratory modulation of S1–S2 interval is also shown for a single subject and for a single respiratory cycle in figure 3.

2.3.3. S1–S1 interval—respiratory sinus arrhythmia. RSA is normally defined as the variation in R–R intervals in the ECG caused by respiration and is a well-known neurophysiological phenomenon (Berntson *et al* 1993).

The presence of a central cardio-pulmonary rhythm generator—arising in the Nucleus Tractus Solitarious—causes the heart-rate to vary at typical respiratory frequencies even in the absence of respiratory mechanisms. This occurs primarily through a central vagal drive and a sympathetic generator that affect vagal and sympathetic motor neurons respectively. The vagal effects have been found to strongly outweigh the sympathetic processes due to the inherently slower responses of the latter and their inability to keep up with the drive frequencies.

Berntson *et al* report that respiration has an overlaying effect, quite like 'phasic modulation' or 'gating,' on central heart-rate variability. This respiration-dependent modulation is reported to be caused by peripheral afferents, such as baroreceptors, chemoreceptors and cardio-pulmonary stretch receptors. For instance, the inhibition of baroreceptor and chemoreceptor reflexes during inspiration leads to reduced vagal drive, resulting in an increased heart-rate during the inspiratory phase. Coleridge and Coleridge (1991) report that afferent cardio-pulmonary stretch receptor reflexes, associated for instance with the respiratory inflation and deflation of the lungs, similarly contribute to respiration-dependent modulations in vagal outflow and, consequently, in heart-rate.

While the interval between the R wave and S1 is also modulated by respiration to some extent, this modulation is relatively small (an average of 12 ms as reported in Sakamoto (1965)), and its variation from beat to beat is even smaller. The S1–S1 interval is, therefore, also expected to reflect RSA closely.

As shown in figure 9, S1–S1 interval measured using the accelerometer was found to be lowered during inspiration corresponding to elevated heart-rate during the inspiratory phase; and conversely, S1–S1 interval measured during expiration was found to increase corresponding to reduced heart-rate. As such, the SCG-derived S1–S1 interval was found to show respiratory trends congruent with physiological mechanisms of RSA.

2.4. SCG changes during apnea

As shown in figure 9, each of the three SCG parameters shows statistically significant changes ($p < 0.05$, corrected for multiple comparisons based on the Holm–Bonferroni method) during an interval of apnea when compared to each of the four respiratory phases—start inspiration, peak inspiration, start expiration and peak expiration.

Additionally, for the 18 subjects, during the interval of apnea, statistically significant differences were observed between the three SCG parameters themselves—S1–S2 interval, S1–S2 power ratio, and S1–S1 interval. Among the three SCG parameters, S1–S2 interval showed the lowest mean amplitude during apnea, across the 18 subjects, when normalized to the duration of recording for each individual time trace. This was congruent with the relatively flat S1–S2 interval trace for an individual subject, as shown in figure 6. The mean amplitude (normalized) of the S1–S2 power ratio was higher during apnea as compared to the mean amplitude (normalized) of the S1–S2 interval, in accordance with the power of the S2 heart

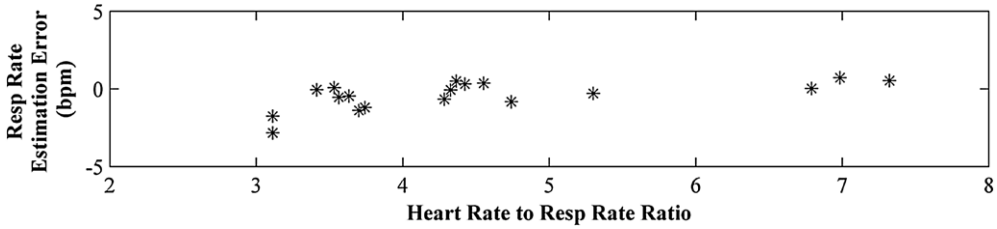

Figure 10. Difference between respiration rates, as derived from the combined accelerometer parameters and the reference respiration belt, plotted as a function of the ratio of heart-rate and respiration-rate, across 18 subjects.

sound being lower than the power of the S1 heart sound during apnea (figure 6). Finally, the mean amplitude (normalized) of the S1–S1 interval was found to be the highest among the three parameters. This was congruent with the physiologically-expected Valsalva-like drastic increase followed by slow decrease of S1–S1 interval during apnea (figure 6).

2.5. Effects of heart-rate on respiration-rate estimation

Shown in figure 10 is the performance of the accelerometer-based respiration-rate measurement approach when compared to a reference respiration belt as a function of heart-rate to respiration-rate (HR:RR) ratio for all 18 subjects. It is noteworthy that, for this measurement dataset, this ratio does not fall below two, hence the sampling rate is always above the Shannon–Nyquist sampling limit (Shannon 1949, Nyquist 1928), making the reconstruction of respiration waveforms less susceptible to the effects of aliasing. No significant trend was observed in the performance of respiration-rate estimation as a function of heart-rate—a Kendall's rank correlation coefficient value of 0.477 was obtained between the heart-rate to respiration rate ratio and the respiration rate estimation error (Kendall 1938).

2.6. Importance of monitoring multiple features

The key advantage of fusing information from multiple SCG features to assess respiration trends and rates is reducing the reliance on any individual parameter that may or may not manifest strong respiration-dependent trends based on inter-subject physiological variability.

The S1–S2 intensity ratio, for instance, would be more susceptible to sensor noise, imprecise sensor placement, vibration pick-up and low levels of motion artifact that may not as adversely impact other parameters such as baseline wander from chest wall motion, or the S1–S1 and S1–S2 intervals, which rely more heavily on the accuracy of S1 and S2 detection, as opposed to beat-powers.

Furthermore, the autonomic feedback loop is known to weaken with age (Hellman 1976), statistically making RSA a poor index for respiration in the elderly population. Also, given that RSA or heart-rate variability in the respiratory frequency band is a complex and combined effect of several central and peripheral processes and factors (physiological, psychological and neurological) (Berntson *et al* 1993), it would not be ideal or robust to rely on RSA-derived respiration as a single metric for respiration, as is the case with some ECG-derived respiration (Cysarz *et al* 2008). Even when ECG-derived respiration uses amplitude information (Moody *et al* 1985), for adequate robustness, multiple ECG leads are required; furthermore, the variation in cardiac axis is highly subject-dependent. Similarly, the respiration-dependent

ultra-low frequency component is known to be easily corrupted by motion artifacts (Pandia *et al* 2010) and postural changes.

An approach that combines features from multiple parameters would yield a more robust respiration measure. Although in this work, one of the metrics—the S1–S2 intensity ratio—yielded the strongest agreement with the respiration belt, in more challenging settings the combination of the metrics could be advantageous. For example, the S1–S2 intensity ratio would be more sensitive to motion artifact than many of the other metrics, since it relies on the amplitude of the waveform, rather than timing intervals. Consequently, in the presence of motion artifact, fusing the information from all of the metrics together with a sophisticated algorithm could improve the overall respiration rate detection. Future work will focus on developing such algorithms for combining the information from each of these features to improve the robustness of respiration monitoring using SCG.

2.7. Limitations of SCG-based respiration monitoring

One limitation of this study is the use of the ECG for the initial detection of the heartbeats. Nevertheless, heartbeat detection could ultimately be performed directly on the SCG signal, using S1-detection methods such as those shown in Pandia *et al* (2010). Alternatively, a chest patch containing both an accelerometer and two or three electrodes for ECG measurement could be developed for recording both the ECG and SCG simultaneously. Another minor limitation is that the calculated S1–S2 interval derived based on the comparison of consecutive beats (as described in 1.4.2) could be impacted adversely if the change in systolic interval between consecutive beats was greater than 30 ms. This could be resolved in future work by increasing the maximum window considered to greater than 30 ms at the expense of computation time. Future work will also investigate the effects of cardiovascular, respiratory and autonomic dysfunction on SCG-based respiration monitoring.

3. Conclusions and future directions

A miniature accelerometer mounted on the chest was configured to measure a seismocardiogram (SCG) signal. The SCG signal is produced, in part, as a result of cardiac events, and is transduced on the skin surface using the accelerometer. This work highlights that over and above valuable cardiac information, the SCG signal also contains respiratory information resulting from cardio-respiratory interactions. Presented here are multiple respiration-dependent parameters extracted from a chest-mounted accelerometer. Further, three respiration-dependent parameters of the SCG signal—intensity modulation of heart sounds, timing interval changes within each heartbeat and timing interval changes between successive heartbeats—were used here to each derive a respiration rate measure. The respiration rate derived from each of the three parameters was found to be in strong agreement, across 18 subjects, with the respiration rate detected from a reference respiration belt.

Furthermore, phase relations of each of the three respiration-dependent parameters of the SCG signal were investigated at four different points along the respiration cycle—start inspiration, peak inspiration, start expiration and peak expiration—for all 18 subjects. The phases of each of the three SCG parameters were found to be congruent with physiologically-expected trends. The waveforms of the SCG parameters were also investigated during breath hold. Statistically significant differences were observed between each of the three parameters during breath hold. Moreover, for each SCG parameter, statistically significant changes were observed during breath hold relative to each of four respiratory phases—start inspiration, peak inspiration, start expiration and peak expiration.

Owing to the relation of these parameters to variables such as blood pressure, autonomic control, physical movement, a next step would be to investigate the phase relations between the respiration signals reconstructed from the different parameters, and the impact of activity and posture on these signals. Of specific interest would be the impact of the autonomic feedback loop on the phase and amplitude of the RSA signal under different conditions that modulate autonomic activity—like the Valsalva maneuver (Lu *et al* 2001) and during exercise recovery (Vallais *et al* 2008). Future work would also include a thorough comparison of accelerometer-derived respiration-rates and waveforms against other accepted references, such as spirometer-derived flow and volume. This approach should also lend itself to the automatic detection and classification of breath hold or apneic events using enhanced signal classification algorithms.

Acknowledgments

The authors would like to thank Dr Stephen Ruoss and Dr Michael Chen for their highly valuable inputs and for very productive technical discussions.

References

Agress C M, Fields L G, Wegner S, Wilburne M, Shickman M D and Muller R M 1961 The normal vibrocardiogram: physiologic variations and relation to cardiodynamic events *Am. J. Cardiol.* **8** 22–31

Amit G, Shukha K, Gavriely N and Intrator N 2009 Respiratory modulation of heart sound morphology *Am. J. Physiol. Heart Circ. Physiol.* **296** H796–805

Berntson G G, Cacioppo J T and Quigley K S 1993 Respiratory sinus arrhythmia: autonomic origins, physiological mechanisms, and psychophysiological implications *Psychophysiology* **30** 183–96

Bland J M and Altman D G 1986 Statistical methods for assessing agreement between two methods of clinical measurement *Lancet* **1** 307–10

Castiglioni P, Faini A, Parati G and Di Rienzo M 2007 Wearable seismocardiography *IEEE Conf. on Engineering in Medicine and Biology Society* pp 3954–7

Coleridge H M and Coleridge J C G 1991 Afferent innervation of lungs, airways, and pulmonary artery *Reflex Control of the Circulation* (Boca Raton, FL: CRC Press) pp 579–607

Cysarz D, Zerm R, Bettermann H, Frühwirth M, Moser M and Kröz M 2008 Comparison of respiratory rates derived from heart rate variability, ECG amplitude and nasal/oral airflow *Ann. Biomed. Eng.* **36** 2085–94

Droitcour A, Seto T, Park B, Yamada S, Vergara A, Hourani C, Shing T, Yuen A, Lubecke V and Boric-Lubecke O 2009 Non-contact respiratory rate measurement validation for hospitalized patients *IEEE Conf. on Engineering in Medicine and Biology Society* pp 4812–5

Hellman J B 1976 Variation of respiratory sinus arrhythmia with age *J. Appl. Physiol.* **41** 734–8

Holm S 1979 A simple sequentially rejective multiple test procedure *Scand. J. Stat.* **6** 65–70

Kendall M 1938 A new measure of rank correlation *Biometrika* **30** 81–9

Kusukawa R 1966 Hemodynamic determinants of the amplitude of the second heart sound *J. Appl. Physiol.* **21** 938–46

Lababidi Z, Ehmke D A, Durnin R E, Leaverton P E and Lauer R M 1970 The first derivative thoracic impedance cardiogram *Circulation* **41** 651–8

Leighton R F 1971 Right and left ventricular systolic time intervals: effects of heart rate, respiration and atrial pacing *Am. J. Cardiol.* **27** 66

Lim W S, Carty S M, Macfarlane J T, Anthony R E, Christian J, Dakin K S and Dennis P M 2002 Respiratory rate measurement in adults—how reliable is it? *Respir. Med.* **96** 30–3

Lu K, Clark J W Jr, Ghorbel F H, Ware D L and Bidani A 2001 A human cardiopulmonary system model applied to the analysis of the Valsalva maneuver *Am. J. Physiol. Heart Circ. Physiol.* **281** H2661–79

Messer S 2001 Optimal wavelet denoising for phonocardiograms *Microelectron. J.* **32** 931

Moody G B, Mark R G, Zocola A and Mantero S 1985 Derivation of respiratory signals from multi-lead ECGs *Comput. Cardiol.* **12** 113–6

Morillo D S, Ojeda J L R, Foix L F P and Jimenez A L 2010 An accelerometer-based device for sleep apnea screening *IEEE Trans. Inform. Technol. Biomed.* **14** 491–9

Nyquist H 1928 Certain topics in telegraph transmission theory *Trans. Am. Inst. Electr. Eng.* **47** 617–44

Pandia K, Ravindran S, Cole R, Kovacs G T A and Giovangrandi L 2010 Motion artifact cancellation to obtain heart sounds from a single chest-worn accelerometer *ICASSP: IEEE Int. Conf. on Acoustics Speech and Signal Processing (Dallas, TX)* pp 590–3

Reinvuo T, Hannula M, Sorvoja H, Alasaarela E and Myllyla R 2006 Measurement of respiratory rate with high-resolution accelerometer and emfit pressure sensor *Proc. IEEE Sensors Applications Symp.* pp 192–5

Sakamoto T 1965 Hemodynamic determinants of the amplitude of the first heart sound *Circ. Res.* **16** 45

Salerno D M and Zanetti J M 1991 Seismocardiography for monitoring changes in left ventricular function during ischemia *Chest* **100** 991–3

Savitzky A and Golay M J E 1964 Smoothing and differentiation of data by simplified least squares procedures *Anal. Chem.* **36** 1627–39

Shannon C E 1949 Communication in the presence of noise *Proc. IRE* **37** 10–21

Tavakolian K, Ngai B, Blaber A P and Kaminska B 2011 Infrasonic cardiac signals: complementary windows to cardiovascular dynamics *IEEE Conf. on Engineering Medical Biology Society* 4275–8

Tavakolian K, Vaseghi A and Kaminska B 2008 Improvement of ballistocardiogram processing by inclusion of respiration information *Phys. Meas.* **29** 771–81

Vallais F, Lucini D, Pagani M and Baselli G 2008 The synchrony between baroreflex sequences and cardio-respiratory activity *Comput. Cardiol.* **35** 809–12

Woodward S H, Arsenault N J, Voelker K, Nguyen T, Lynch J, Leskin G and Sheikh J 2007 Estimating heart rate and RSA from the mattress-recorded kinetocardiogram *Psychophysiology* **44** 635–8

Zanetti J M and Salerno D M 1991 Seismocardiography: a technique for recording precordial acceleration *IEEE Symp. on Computer Based Medical Systems* pp 4–9